Biosensors and Bioelectronics 128 (2019) 37–44

Contents lists available at ScienceDirect

Biosensors and Bioelectronics

journal homepage: www.elsevier.com/locate/bios

Detection of apoptotic and live pre-osteoblast cell line using impedance-based biosensors with variable electrode design

A. Gabriela Montaño-Figueroa[a,b], Sutton E. Wheelis[c], Brian M. Hedden[c], Niman H. Alshareef[b], Dheera Dammanna[b], Hana Shaik[b], Danieli C. Rodrigues[c], Manuel Quevedo-Lopez[a,b,*]

[a] Departamento de Investigación en Polímeros y Materiales, Universidad de Sonora, Rosales y Luis Encinas, Hermosillo, Sonora 83000, Mexico
[b] Department of Materials Science and Engineering, The University of Texas at Dallas, Richardson, TX 75080, USA
[c] Department of Bioengineering, The University of Texas at Dallas, Richardson, TX 75080, USA

ARTICLE INFO

Keywords:
Electrode diameter/configuration
Cell spreading
Apoptosis
EIS
Impedance-based biosensors

ABSTRACT

Electrical impedance-based sensing of cell activity has become a powerful analytical tool that allows the monitoring of several relevant biological processes associated with cell evolution and morphology. In these types of biosensors, the electrode design has a direct impact on the sensitivity because it defines the capability of the biosensor to measure small changes in the impedance resulting from cell activities. Herein, impedance-based biosensors arrays with several configurations were successfully developed and used to study the impact of the electrode layout on the dynamics of cultured pre-osteoblast cells. The biosensor design was initially validated by measuring the effect of electrode design on the capacitance of a dielectric polymer (parylene) that mimics the dielectric characteristics of cell populations, results are shown in the Supplementary information section. Results from *in vitro* cell growth indicate that the optimized design of single electrodes with a diameter of 50 μm, are the most sensitive to cell motion whereas increasing the number of electrodes allows clear differentiation between living and dead cells after 3 h of inducing apoptosis. Apoptosis death was induced with Staurosporine, a chemical mediator of apoptosis in osteoblasts. These impedance results have been validated with optical imaging and flow cytometry analysis that were performed on parallel cultures. Frequency and electrolyte concentration effects are also discussed.

1. Introduction

Interest in the development of biosensors that are compatible with established chip microfabrication processes has reached unprecedented levels. This will allow miniaturization of many types of biosensors and allow their integration with microelectronics and Micro-Electro-Mechanical Systems (MEMS) circuits and on-chip micro-power units that can be wearable, epidermally attached, or even implantable. An ideal biosensor is expected to have several key features including high sensitivity, label-free procedures, non-invasiveness, real-time response, automation, and portability. Among them, impedance-based cell analytical methods are becoming one of the most important techniques for biosensing, (Pancrazio et al., 1999; Thomas et al., 1972) and have been greatly improved thanks to the development of nanotechnology and interfacing between sensors and cells (Radke and Alocilja, 2005). In particular, these biosensors have been proven to be powerful tools to monitor various cell types under different experimental conditions. Some of these include: cell shape (Arndt et al., 2004; Keese and Giaever, 1994; Tiruppathi et al., 1992), cell life cycle (Zhu et al., 2015), cytotoxicity (Asphahani et al., 2012; Pancrazio et al., 2003; Ramis et al., 2013; Yeon and Park, 2005), as well as cell motility (Luong et al., 2001) and micromotion (Lovelady et al., 2009). They have also been widely extended to include more diverse fields, such as the study of virus-induced cell membrane fusion (Watterson et al., 2016) and food safety monitoring through pathogenic bacteria detection (Radke and Alocilja, 2005).

Generally, impedance-based biosensors fabricated on a substrate with integrated electrodes can have either an interdigitated electrode (IDE) or a structure consisting of small detecting electrode surrounded by a large counter electrode (See S1a-b in the Supplementary material file). The latter is the most conventional layout because it offers the possibility of different electrode configurations where one or multiple electrodes can be used. The use of multiple electrodes allows the decoupling of electrodes from the number of contact pads and more sensing areas to be in contact with the cells, unlike individual electrodes, which are always limited by the number of available contact

* Corresponding author at: Department of Materials Science & Engineering, The University of Texas at Dallas, Richardson, TX 75080, USA.
E-mail address: mquevedo@utdallas.edu (M. Quevedo-Lopez).

https://doi.org/10.1016/j.bios.2018.11.057
Received 27 August 2018; Received in revised form 22 November 2018; Accepted 23 November 2018
Available online 27 December 2018
0956-5663/

pads (Obien et al., 2014) (See S1c in the Supplementary material file). Briefly, the premise behind the use of these substrate-integrated electrodes configurations relies upon the fact that biological cells behave as dielectric particles when they are immersed in culture media and subjected to a small voltage signal, due to the lipid bilayer plasma membrane, and function to restrict (or impede) the flow of the current. Thus, when the cells attach to and spread over the planar metal electrodes, they impede the current flow from one electrode into the bulk electrolyte and alter the impedance of the biosensor device (Giaever and Keese, 1993; Keese and Giaever, 1994; Lo et al., 1995; Maxwell, 1954; Stolwijk et al., 2015; Wegener et al., 2000).

It is well known that electrode layout is a critical factor that must be considered when developing impedance-based biosensors since this can directly affect the electrical responses of the sensors. However, little attention has been given to the direct impact of various electrodes sizes and configurations on the biological processes relevant for anchorage-dependent cells, such as pre-osteoblasts. By better defining the best electrode size/arrangement, the quality and accuracy of the information will improve and therefore, a more accurate analysis could be generated. Our paper demonstrates a novel electrode configuration different to those discussed above and specifically addresses two aspects of this area of research. First, the paper shows a novel impedance-based biosensor designed to electrically detect and monitor living, apoptotic/necrotic pre-osteoblast cells in tissue cultures through different detecting electrode configurations. Second, an optimal electrode size and configuration for the detection of pre-osteoblasts using the biosensor is investigated. Finally, cell activities such as cell spreading, detachment, and death were monitored using our biosensor in parallel with other means such as optical microscopy and flow cytometry analysis.

2. Materials and methods

2.1. Coplanar electrode array design and micro fabrication process

The substrate integrated electrode arrays designed for this study have a unique combination of different circular electrode diameters of approximately 50, 150 and 250 μm and two large rectangular counter electrodes. Each electrode size was arranged either as an individual electrode or as multiple detecting electrodes fabricated in parallel on the same glass substrates. All electrode arrangements are listed in Table 1. The fabrication process, shown in Fig. 1, began with standard lift-off photolithography process to pattern the electrodes onto glass substrate (76 × 52 mm, with a thickness of approx. 1 mm). After spin-coating and patterning a positive photoresist (S1813) layer, a chromium thin film (200 nm) was evaporated on the patterned photoresist on substrate. Subsequently, a lift-off process was performed with acetone, which removes the photoresist, but leaves the chromium metal patterns. A hafnium oxide (HfO_2) insulating layer (10 nm thick) was grown by atomic layer deposition (ALD), followed by 1000 nm of silicon oxide (SiO_2) deposited by plasma-enhanced chemical vapor deposition (PECVD). The SiO_2/HfO_2 bilayer covered the entire substrate. A second photolithography step was performed to define the active sensing areas exposing the detecting electrode, counter electrode, and contact pads. The device was then baked at 115 °C for 5 min, followed by etching of the SiO_2/HfO_2 bilayer by submerging the device in a buffered oxide etch (BOE 7:1) solution for three minutes. After that, the device was cleaned in acetone to remove any debris and the remaining photoresist, followed by isopropanol (IPA) and deionized water (DIW). Finally, a last lift-off photolithography process was used to pattern 200 nm of a gold layer deposited by e-beam evaporation on top of the electrodes. The device was then cleaned by ultrasonication in acetone, IPA, and DIW for five minutes each, and then dried under nitrogen flow. Au electrodes were selected because of its good conductivity and biocompatibility. Before testing, a fast-cure silicone biocompatible glue (MEDI-4213, Nu-Sil Technology, USA) was used to affix a 3D printed plastic culture well onto the device so that the detecting electrodes could be in contact with the different solutions during impedance measurements.

Table 1
Electrode configuration including individual and multiple detecting electrodes.

Electrode type	Detecting electrode diameter (μm)	Detecting electrode area $(\mu m)^2$	Counter electrode area $(mm)^2$	Sample code
Individual	50	1963.4	17,380	I-50 μm
Individual	150	17,671.4	17,380	I-150 μm
Individual	250	49,087.3	17,380	I-250 μm
Multiple	50	68,719	17,380	M-50 μm
Multiple	150	106,028.4	17,380	M-150 μm
Multiple	250	294,523.8	17,380	M-250 μm

As seen in Table 1, the area of the detecting electrodes, either individual or multiple type, is small compared with that of the counter electrode. With this configuration, the impedance of the latter becomes negligible and the impedance of the detecting electrodes dominates the measurement.

2.2. Pre-osteoblasts: cell culture protocol

Murine pre-osteoblasts (MC3T3-E1) (American Type Culture Collection, Manassas, VA, USA) were cultured on the surface of the different electrode configurations, to evaluate the changes in the impedance due to cell growth. Prior to the experiment, pre-osteoblasts were cultivated in T-75 flasks until confluent at 37 °C and 5% CO_2 in Alpha Minimum Essential Medium (αMEM, Hyclone, Logan, UT). Culture media was supplemented with 10% Fetal Bovine Serum (FBS) (HycloneTM, Logan, UT) and 1% Penicillum-Streptomycin (10,000 U, mL) (Gibco, Thermofisher Scientific Waltham, MA). Before seeding, the devices were ultraviolet sterilized for 1 h. To accommodate the culture media volumes a plastic culture well was glued on top of the electrodes area with an approximate size of 8 × 12 × 15 mm (electrolyte reservoir). The biosensors devices were inoculated with a density of 30,000 cells per well. Culture media was added to each sensor to bring the total well volume up to 500 μL and 500 μL of only culture media were added to other biosensors as controls. All the devices were incubated and then measured at different time points (0, 3, 6, 24, 27, and 30 h). A different set of biosensors were used at each time point to prevent cell disruption and death during the measurement. Specific time points also had corresponding optical microscopy (OM) measurements, where cells were imaged using a Keyence VHX 2000 optical microscope to visualize cell growth and attachment (Keyence, Osaka, Tokyo, Japan). All experiments were performed in triplicates at each time point (n = 3), with a total of 216 samples.

2.2.1. Induction of apoptosis on electrode arrays via Staurosporine

To study the difference between viable and dead cells in terms of electrical impedance, a different experiment was conducted where an apoptotic response was intentionally induced using a well-known chemical reagent, called Staurosporine (STS) (Abcam, Cambridge, UK), which is known to be an effective osteoblast apoptogen (Antonsson and Persson, 2009; Grigoriou et al., 2005). A stock solution of 100 nM was prepared by dissolving STS (1 mM) in culture media (αMEM) to induce apoptosis. Impedance cell-based biosensors were then inoculated with the same cell density per well as before and incubated for 24 h to allow adherence to the electrode surfaces under standard culture conditions. After this time, the culture media was then replaced with 750 μL of the culture media supplemented with STS, and electrical measurements were taken at different times points (0, 1, 2, 3, 12 and 24 h). The culture medium with different compositions (αMEM supplemented and not supplemented with STS) and living cells were used as controls for each time point.

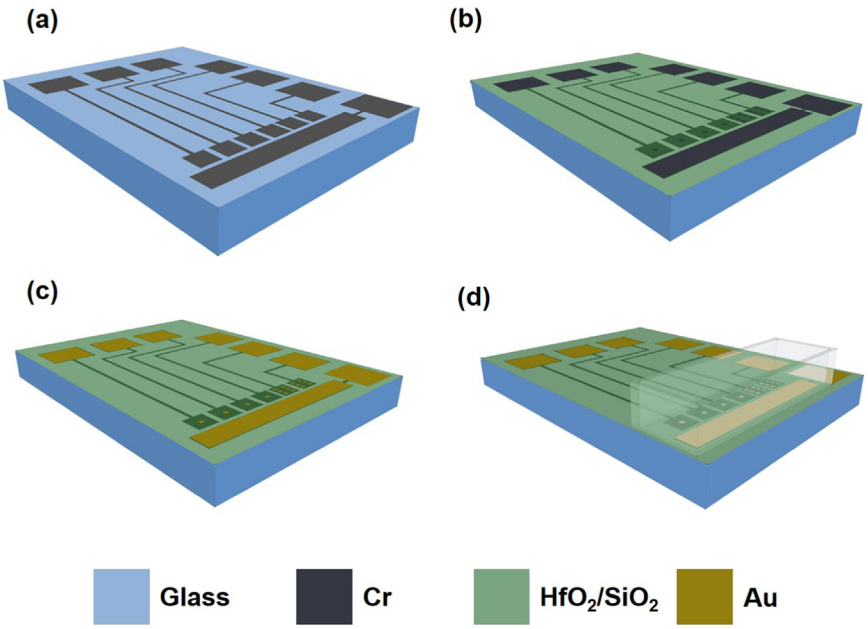

Fig. 1. Schematic representation of the impedance-based cell biosensor. Fabrication consisted of a) evaporation of 200 nm chromium metal electrodes onto glass substrates and patterned by a lift-off process; b) growth of an insulating layer made of HfO_2/SiO_2 by ALD and PECVD, respectively and patterning of the insulating layers by wet etching process, c) deposition of 200 nm gold layer by e-beam evaporation and patterning by a lift-off process, and finally d) attachment of a plastic well (electrolyte reservoir) on top of the devices to contain the culture media and the cells in the right area (detecting/working electrodes area); the metal parts were not in contact nor touched by the well to avoid biosensing capacity compromising during measurements. Both the plastic and the glue used are biocompatible.

2.3. Impedance measurements

The electrodes were connected in a two-electrode configuration and the impedance of the device was measured in the frequency range of 20 Hz to 1 MHz, using an AC voltage of 50 mV amplitude. No DC bias was applied across the detecting and counter electrodes. Impedance was recorded with an Agilent® LCR-meter. The complex impedance was calculated using:

$$Z_w = \frac{U_w}{I_w} = Z_{RE} + jZ_{IM}$$

where j is the imaginary number and ω is angular frequency. The real (Z_{RE}) and the imaginary (Z_{IM}) parts of the complex impedance are called resistance and reactance, respectively. The magnitude of the impedance was then calculated using:

$$|Z| = \sqrt{(Z_{RE})^2 + (Z_{IM})^2}$$

Three replications for each data time point were tested. All biosensors were assumed to have the same physical properties. Each experiment was conducted on a different biosensor array and no pretreatment of the sensor with adhesive support (components of the extracellular matrix) was necessary for the cells, so it was guaranteed that no additional stimulation of the cells occurs. Negative controls were also measured (culture media (αMEM) and the culture media supplemented with STS (αMEM + STS)).

2.4. Apoptosis detection by flow cytometry with Annexin V/FITC-PI

The induction of apoptosis with the STS media was corroborated by flow cytometry analysis through an Annexin V-FITC/PI kit (Abcam, Cambridge, UK). Typically, once apoptosis is induced, the cell membrane translocates an inner phospholipid phosphatidylserine (PS) to the outer layer while preserving the membrane structure and preventing impermeable dyes, like propidium iodide (PI), from entering the cell. Annexin V has a strong binding affinity to PS and is usually conjugated with a fluorescent dye such as fluorescent isothiocyanate (FITC) to identify the early stages of apoptosis. The assay was performed according to the manufacturer's instructions and an LSR Fortessa Flow Cytometer (BD Biosciences, San Jose, CA, USA) was used to analyze the Annexin V-FITC binding, which was excited (Ex) at 488 nm. The emission fluorescence (Em) was collected at 530 nm using a FITC signal detector and PI staining by the phycoerythrin emission signal detector. Propidium iodide was excited at 535 nm and the emission fluorescence was collected at 617 nm. Single stain colors were used as compensation controls during the analysis with FlowJo software (LLC, Ashland, OR, USA).

3. Results and discussion

This paper has two primary objectives: a) the development of an impedance-based biosensor for the continuous measurement of pre-osteoblasts by investigating the impact of electrode configuration on living, apoptotic/necrotic cells; and b) determine an optimal electrode size and configuration for the detection of different cell dynamics of the cultured pre-osteoblasts.

A separate approach using parylene coatings on the surface of the electrodes in different percentages was used to validate our sensor concept and operation, and capacitance measurements were used as an indirect measure of the sensor sensitivity. Results are shown in the Supplementary material S3a–c.

3.1. Impact of electrode size and geometry on impedance-based sensor functionality

A cell culture was conducted on the surface of the detecting electrode configurations, and the data obtained is shown in Fig. 2. Here, pre-osteoblasts were inoculated at time zero, and the impedance values were recorded at 0, 3, 6, 24, 27 and 30 h. In Fig. 2a–c bode magnitude plots were generated for each electrode size and their respective arrangement as an individual electrode or multiple electrodes. In general, a clear difference between individual and multiple detecting electrodes was demonstrated for all configurations. Individual electrodes exhibit higher impedance, whereas a combination of them will result in lower impedance values, because the latter offers more pathways for the current to follow. It can be also noted that the value of the impedance decreased inversely with the area of the electrodes. One of the advantages of using multiple small electrodes is an increase of the detection total area per contact pad, sensing more cells at the same time, and therefore, providing a more general analysis for a larger cell population. In all the cases, almost no change over time can be observed, over the frequency range tested. Nonetheless, if a single frequency is selected when monitoring the activity of the cells, the changes in the

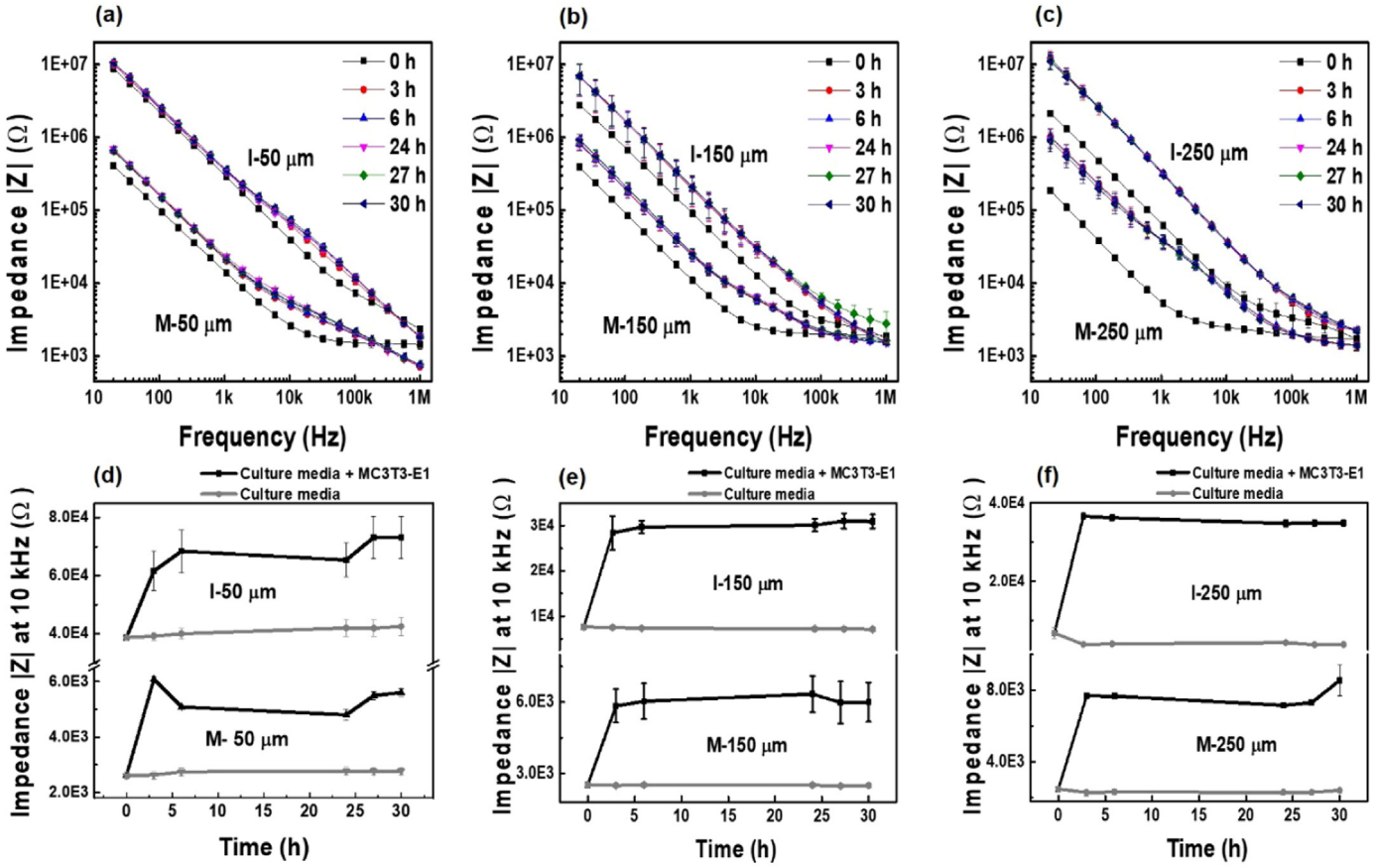

Fig. 2. Electrode arrangement impact on cell culture of pre-osteoblasts. Bode magnitude plots for each electrode size and their respective arrangements as an individual and multiple of a) 50, b) 150, and c) 250 µm diameter; Magnitude of the impedance at 10 kHz as a function of the time for individual and multiple electrodes of d) 50, e) 150, and f) 250 µm diameter.

magnitude of the impedance over time can be clearly seen, as depicted in Fig. 2d–f. Different frequencies were found with maximum sensitivities in the range of 1–18 kHz for each detecting electrode diameter/configuration, where the largest cell-to-baseline changes in the measured impedance were generated, however the optimal measurement frequency selected in this study was 10 kHz and to make fair comparisons between the different detecting electrode arrangements, all the graphs were plotted at this frequency. The reason for the impedance changes is most likely the presence of the cells on the surface of the detecting electrodes and the dielectric properties of their cell membranes, that are partially or totally blocking the area of the detecting electrode that was available for current to flow, a conclusion that is corroborated by the fact that no change in impedance is observed over time when just the culture media was measured (controls). Once the pre-osteoblasts started to drift downwards, they attached to the electrodes in a time-dependent manner. The measured impedance continued to change with minor fluctuations because of the cells being alive and in motion. In all the electrode configurations and sizes, the magnitude of the impedance increased very rapidly at first and then approached a steady-state, normally within 3 h post-inoculation for the detecting electrodes with a diameter of 150 and 250 µm, regardless of electrode configurations. In the case of I-50, the steady-state was seen at about 6 h instead. Nevertheless, the biosensor proved a very high sensitivity by distinguishing cell events within the first hours of cell growth, even though just a few cells were in contact with the electrodes areas. Smaller detecting electrodes can be expected to have better detection sensitivity toward motion of cells, due to their unique ability to detect small populations of cells that adhere to the electrode surface areas as compared to bigger electrodes. Circular I-50 µm has an area similar to that of a single pre-osteoblast cell, which indicates the capability of that electrode to record individual cell responses. The detecting electrode diameter impacted the magnitude of the impedance response and can be explained in terms of the phase angle (θ) that was also measured for all the detecting electrodes submerged in culture media (See Supplementary information S2a). At the low frequency end and irrespective of the arrangement studied, the phase angle was around $\theta = -81$ to -73°, whereas at the high frequency end the phase angle was near to zero in the case of individual electrodes. The low frequencies phase values indicate a capacitive charging process happening at the electrodes surfaces, the so-called double layer capacitance. For individual electrodes this capacitive behavior is displaced to higher frequencies as the diameter was reduced and a combination of capacitance and resistance processes at the middle range of frequencies for multiple electrodes, whereas just the resistive part dominates at high frequencies region ($\theta = 0^{\circ}$).

It can be assumed the measured impedance would continue to increase with minor fluctuations until reaching an upper limit (value for a confluent cell layer) if the cells remained viable and firmly attached to the electrode surfaces, varying according to the electrode diameter and arrangement. However, the cell culture time was limited to 30 h during this assay.

3.2. Optical microscopy and normalized Impedance

Following seeding, anchorage-dependent cells such as pre-osteoblasts are expected to undergo morphological changes (Chae et al., 2000; Grigoriou et al., 2005; Wyllie et al., 1980). In this study, those changes were monitored through optical microscopy of the wells at different time points as shown in Fig. 3. At t = 0, the cells were in suspension and appeared spherical. Optical images taken 3 h after

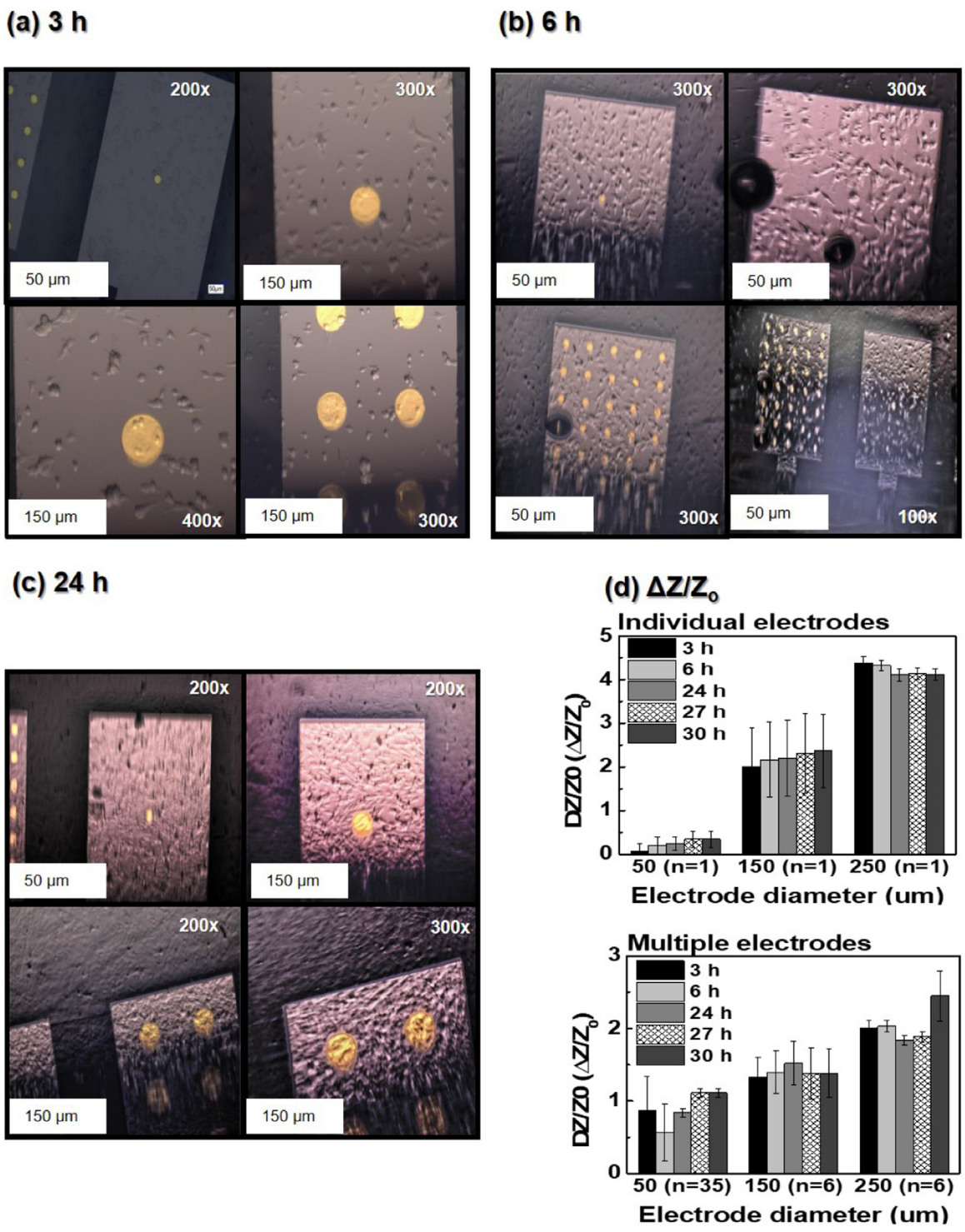

Fig. 3. Cell morphology analysis through optical microscopy. Different electrode diameters at a) 3 h, b) 6 h, and c) 24 h after cell inoculation and d) normalized impedance of individual electrodes (upper panel) and multiple electrodes (lower panel).

seeding, shown in Fig. 3a, confirmed the cells were attaching to the surfaces and appeared slightly more branched in their morphology, this provoked a very rapidly increment of the impedance, even though just a few cells were on the surface of the different electrodes. The shape of the cells turned to flattened forms with larger dimensions from their initial circular form, and can be seen in Fig. 3b, after 6 h post-inoculation. According to these results, the considerable change in cell shape referred to as cell spreading took place within the first hours of cell growth. The optical images shown in Fig. 3c confirmed favorable growth conditions, by demonstrating cell adhesion and spreading, possibly due to the development of focal adhesions and stress fibers. Pre-osteoblasts showed significant differences in cell area and morphology, crowding the bottom of the biosensor, regardless of the type of detecting electrode and proving a generation time of approximately 24 h. The changes in the impedance over time shown in Fig. 2e–f are directly correlated with the changes in the shape of cultured cells at the different time points, but is more evident for the I-50 µm which demonstrates the strength of this technique to monitor changes in

morphology and cell spreading using small detecting electrodes.

The effect of the electrode size and arrangement on sensor sensitivity was demonstrated with the normalized impedance shown in Fig. 3d for individual electrodes (upper panel) and multiple electrodes (lower panel) at 10 kHz. The impedance contributions of the electrode-electrolyte interface and culture media on the total impedance of the biosensor device are not relevant to that of the cells and are considered as the base impedance, expressed as Z_0. The important part of the impedance is caused by cells at a time *t* after adding them to the sensor and is represented by Z_T. This part of the impedance (Z_T-Z_0) obtained from the impedance with cells is usually normalized (Z_T-Z_0)/Z_0 (Martinez et al., 2017; Xu et al., 2016). The normalized impedance is then given by the following expression:

$$Z_{norm} = \frac{Z_T - Z_0}{Z_0} = \frac{\Delta Z}{Z_0}$$

Based on the verification of the cell growth on the detecting electrodes by optical microscopy, an increase of the normalized impedance was expected for the three different electrode sizes/arrangements. Comparing individual electrodes, as the area of the electrode was reduced from almost 50,000–1,963 μm^2, the normalized impedance was also reduced. The difference between the normalized impedances values among the different electrode sizes can be explained in terms of numbers of cells hosted by their surface electrode areas. The I-250 μm electrode has more cells attached to its surface and therefore, the higher value for normalized impedance, which means the contribution of the cell layer to the overall impedance of the biosensor device is higher than the other electrodes. The steady state was reached earliest for the biggest electrode, which reduced the possibility of distinguishing further events, such as cell spreading or cell motion throughout the duration of the cell growth. However, an increasing linear trend can be noticed when the two smallest electrodes are used (I-50 μm and I-150 μm), and there is a good correlation between the different cell stages shown in the optical pictures and the normalized impedance values obtained. By using multiple detecting electrodes arranged in parallel, the normalized impedance changed in the same way for the three electrode configurations. A fluctuation pattern can be seen throughout the different time points and can be attributed to the cell motion on top of the electrodes as previously explained. Small changes happening at the surface of one of the multiple electrodes did not greatly affect the global impedance of the biosensor device because each detecting electrode contributed equally to the overall magnitude of the impedance.

3.3. Electrical, optical and biochemical evaluation of staurosporine-triggered apoptosis

Apoptosis, a highly regulated process that occurs naturally to eliminate damaged cells and maintain constant cell numbers can be triggered by external substances. Staurosporine-triggered apoptosis was investigated on pre-osteoblasts exposed to the drug for 1, 2, 3, 12 and 24 h by sensing the changes in the magnitude of the impedance of all the different types of electrolytes or testing solutions involved in the process as shown in Fig. 4a, using the I-50 μm and M-50 μm electrodes due to the size of the pre-osteoblasts cells, which are typically around 30 μm in diameter, to allow for comparable sizes. A single bode plot curve was generated for each type of electrolyte (not shown). From the bode plot curves 24 h after the addition of the STS media, three frequencies (6, 10, and 100 kHz) were selected and plotted as a function of the different electrolytes for individual electrodes and multiples electrodes (upper panel). Immediately, it can be noted that the impedance is dependent on both the frequency and type of testing solution. It has been reported that at low frequencies, the electrical current will follow a path by the cell surroundings but at the high-frequencies, the electrical shielding effect of the cells is overcome (Giaever and Keese, 1993; Lo et al., 1995). For the range of frequencies used in this study, relatively high frequencies (100 kHz) showed almost no change in impedance with respect to either cell behavior or type of culture media used, which can be seen for both electrode arrangements. This is because the impedance at the high-frequency end is largely dominated by the solution resistance. The effect of cells attached to the surface of the detecting electrodes is reduced due to the relaxation of the dipole species. Also, it is suspected that the impedance caused by the double layer capacitance and the parasitic capacitance is minimized at high frequencies, resulting in a convergence of the impedance towards the resistance of the testing solution, indicated by their phase shift values (See S1a in Supplementary material file) (Radke and Alocilja, 2005).

To better illustrate the variation among the different testing solutions, the impedance response at 10 kHz for I-50 μm and M-50 μm over time is presented in Fig. 4a in the lower panel. A distinctive difference between living and apoptotic cells can be noted according to their impedance curves over time. The decline in the magnitude of the impedance indicates cell death or cell detachment from the electrode or both and is distinct from the signals coming from the negative controls; though an initial increment in all the controls impedance curves confirmed the major effect on the overall biosensor device behavior caused by small perturbations such as the difference in ionic concentration. The difference above mentioned become more evident 360 min (6 h) after induction of apoptosis when individual detecting electrodes are used, followed by a rapid reduction in impedance. For multiple electrodes, that difference is evident at approximately 180 min (3 h), which indicates a higher sensitivity of these multiple electrodes towards the initial different statuses of the cells. From those plots, an initial increase in the impedance can be noticed within the first hours after the initial exposure, which can be explained by the increase of cell volume (swelling) from apoptotic cells. This is due to the fact that cells under certain physiological and physiopathological conditions have different volume regulation processes that, in the case of apoptosis, are usually a regulatory volume increase due to the intake of osmolytes (Asphahani et al., 2012; Okada et al., 2004). Such volume increments happen before cell fragmentation and shrinkage of the cells.

However, by the end of this experiment, just I-50 μm electrodes followed the decrease tendency of the impedance curve. We note that this might be related with how the adhesion between the cells and the surface occurs. Previous reports have indicated that staurosporine induces apoptosis through the activation of a family of cysteine proteases (caspases) which play an important role in the disruption of focal adhesions, hence causing loss of cell attachment to the ECM (Lee and Ruoslahti, 2005; Schneider and Burridge, 1994; Triplett and Pavalko, 2006). The impedance curves for both types of electrodes did not totally decrease 24 h after the exposure to the drug, which might be indicating the presence of cell bodies on the surface of the electrode, which cell-substrate contacts have not been altered significantly and remained attached to the electrode. The biosensor detects them and therefore, contributed to the general value of the magnitude of the impedance.

At 2, 3, and 24 h, two complementary methods were employed to investigate whether the decline in impedance caused by STS correlated with a change in morphology and a biochemical feature. STS exposure has been demonstrated to be not cytotoxic but with an extraordinary ability to induce morphological changes typical of apoptosis (Chae et al., 2000). These changes almost invariably involve cellular shrinkage and blebbing. Cell responses to the STS were collectively monitored by OM and can be seen in Fig. 4b. The change in morphology and adherence of cells after exposure to STS is evident throughout the optical images taken at 3 h, 12 h, and 24 h after the induction of apoptosis. The advance of the apoptotic process is clearly seen, as most of the cells were almost detached from the electrode surface 24 h after the induction. Consistent with the reduction of the adhesion between the cell and the substrate are the changes to round cellular morphology, cell shrinkage, and eventual lysis, which are common features in both types of cell death: apoptosis and necrosis.

Since cell death can be achieved through two main processes,

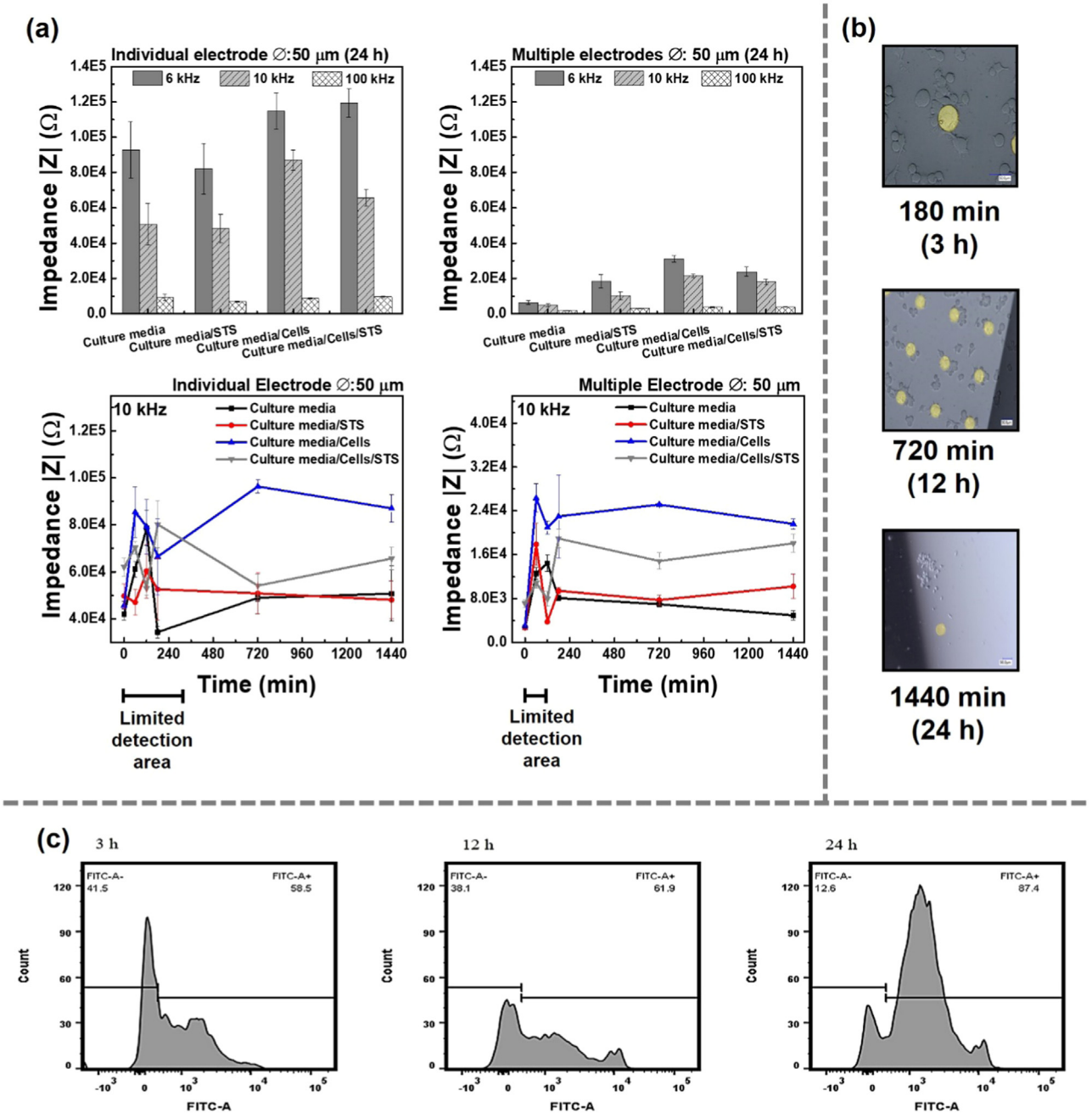

Fig. 4. Apoptosis electrical measurements. a) The magnitude of the impedance as a function of the different testing solutions at 6, 10 and 100 kHz for individual electrodes and multiple electrodes (upper panel). Time course graphs depicting the apoptosis evolution at 10 kHz using individual and multiple electrodes (lower panel). b) Optical imaging of the electrodes at different time points after the induction of apoptosis with STS. c) Flow cytometric analysis of PS by binding of Annexin V-FITC/PI on pre-osteoblasts after 3 h, 12 h, and 24 h of drug (Staurosporine) exposure.

apoptosis and necrosis, that differ morphologically and biochemically (Chae et al., 2000). To confirm cell death by apoptosis, a flow cytometry analysis was performed on the osteoblasts after the exposure to the STS solution, which is known to be an intrinsic apoptosis-triggering chemical reagent. In Fig. 4c, flow cytometry histograms of pre-osteoblasts exposed to STS 100 nM at 3 h, 12 h and 24 h are depicted, showing the analysis of the PS externalization by FITC-Annexin V/PI. Each diagram is separated into two regions, FITC- A- (negative) and FITC- A + (positive). The area of the positive region represents the number of pre-osteoblasts that underwent apoptosis, while that of the negative region denotes the viable or necrotic cells. The apoptosis rate increased as the incubation time with the STS media was increased. 3 h after the exposure to the drug almost half of the cell population appeared to be dead already and finally, almost 87% of the cells were dead within 24 h of the exposure. These results also confirm the cell death through apoptosis obtained with the impedance-cell based biosensors reported here.

4. Conclusions

Impedance-based cell biosensors have been successfully developed for monitoring live and dead pre-osteoblasts. The results reported here proved, that depending on the cell activity to be monitored, a specific electrode configuration must be selected. Single electrodes with the size according to the cell line studied, should be used when an activity such as cell spreading is investigated because these electrodes generated the

most sensitive impedance responses towards cells motions; but in the other hand when the cell activity comes from a collective response from the cells, such as apoptosis, multiple electrodes will give a faster and accurate response, because they could discriminate between a living and a dead cell exactly 3 h after the induction of apoptosis, whereas individual electrodes took longer. The approach of multiple detecting electrodes provides increased cell signal sensitivity when detecting dynamic cellular process, such as the induction of cell death through apoptosis after a drug exposure. Apoptosis was confirmed by flow cytometry, through the analysis of the binding between the PS with Annexin V-FITC/PI with 87% of the cells dead 24 h after the first exposure with STS and by optical images.

In summary, with this work, we are providing the basis for the selection of an electrode configuration that will be application specific, for a more efficient employment of these techniques. Ultimately, the biosensor showed the capability of monitoring cellular dynamics over time, without disrupting the cell monolayer, no need of cell patterning, with data available in real time, automation of the data points and with a very high sensitivity towards detecting morphological alterations of cultured cells.

Acknowledgments

The authors would like to thank The University of Texas at Dallas, the financial support granted by the Consejo Nacional de Ciencia y Tecnología (CONACYT) (Scholarship number 380996) and Rubio Pharma S.A. de C.V..

Declaration of interests

The authors declare that they have no known competing financial interests or personal relationships that could have appeared to influence the work reported in this paper.

Appendix A. Supplementary material

Supplementary data associated with this article can be found in the online version at doi:10.1016/j.bios.2018.11.057.

References

Antonsson, A., Persson, J.L., 2009. Induction of apoptosis by staurosporine involves the inhibition of expression of the major cell cycle proteins at the G2/M checkpoint accompanied by alterations in Erk and Akt kinase activities. Anticancer Res. 29, 2893–2898.

Arndt, S., Seebach, J., Psathaki, K., Galla, H.-J., Wegener, J., 2004. Bioelectrical impedance assay to monitor changes in cell shape during apoptosis. Biosens. Bioelectron. 19, 583–594.

Asphahani, F., Thein, M., Wang, K., Wood, D., Wong, S.S., Xu, J., Zhang, M., 2012. Real-time characterization of cytotoxicity using single-cell impedance monitoring. Analyst 137, 3011–3019. https://doi.org/10.1039/c2an16079j.

Chae, H.J., Kang, J.S., Byun, J.O., Han, K.S., Kim, D.U., Oh, S.M., Kim, H.M., Chae, S.W., Kim, H.R., 2000. Molecular mechanism of staurosporine-induced apoptosis in osteoblasts. Pharmacol. Res. 42, 373–381. https://doi.org/10.1006/phrs.2000.0700.

Giaever, I., Keese, C.R., 1993. A morphological biosensor for mammalian cells. Nature 366, 591–592. https://doi.org/10.1038/366591a0.

Grigoriou, V., Shapiro, I.M., Cavalcanti-Adam, E.A., Composto, R.J., Ducheyne, P., Adams, C.S., 2005. Apoptosis and survival of osteoblast-like cells are regulated by surface attachment. J. Biol. Chem. 280, 1733–1739. https://doi.org/10.1074/jbc.M402550200.

Keese, C.R., Giaever, I., 1994. A biosensor that monitors cell morphology with electrical fields. IEEE Eng. Med. Biol. Mag.

Lee, B.-H., Ruoslahti, E., 2005. α5β1 integrin stimulates Bcl-2 expression and cell survival through Akt, focal adhesion kinase, and Ca2 + /calmodulin-dependent protein kinase IV. J. Cell. Biochem. 95, 1214–1223.

Lo, C.M., Keese, C.R., Giaever, I., 1995. Impedance analysis of MDCK cells measured by electric cell-substrate impedance sensing. Biophys. J. 69, 2800–2807. https://doi.org/10.1016/S0006-3495(95)80153-0.

Lovelady, D.C., Friedman, J., Patel, S., Rabson, D.A., Lo, C.-M., 2009. Detecting effects of low levels of cytochalasin B in 3T3 fibroblast cultures by analysis of electrical noise obtained from cellular micromotion. Biosens. Bioelectron. 24, 2250–2254. https://doi.org/10.1016/j.bios.2008.09.033.

Luong, J.H., Habibi-Rezaei, M., Meghrous, J., Xiao, C., Male, K.B., Kamen, A., 2001. Monitoring motility, spreading, and mortality of adherent insect cells using an impedance sensor. Anal. Chem. 73, 1844–1848.

Martinez, J., Montalibet, A., McAdams, E., Faivre, M., Ferrigno, R., 2017. Effect of electrode material on the sensitivity of interdigitated electrodes used for electrical cell-substrate impedance sensing technology. Conf. Proc. IEEE Eng. Med. Biol. Soc. 2017, 813–816. https://doi.org/10.1109/EMBC.2017.8036948.

Maxwell, J.C., 1954. Electricity and Magnetism.

Obien, M.E.J., Deligkaris, K., Bullmann, T., Bakkum, D.J., Frey, U., 2014. Revealing neuronal function through microelectrode array recordings. Front. Neurosci. 8, 423. https://doi.org/10.3389/fnins.2014.00423.

Okada, Y., Maeno, E., Shimizu, T., Manabe, K., Mori, S.-I., Nabekura, T., 2004. Dual roles of plasmalemmal chloride channels in induction of cell death. Pflug. Arch. 448, 287–295. https://doi.org/10.1007/s00424-004-1276-3.

Pancrazio, J.J., Gray, S.A., Shubin, Y.S., Kulagina, N., Cuttino, D.S., Shaffer, K.M., Eisemann, K., Curran, A., Zim, B., Gross, G.W., O'Shaughnessy, T.J., 2003. A portable microelectrode array recording system incorporating cultured neuronal networks for neurotoxin detection. Biosens. Bioelectron. 18, 1339–1347.

Pancrazio, J.J., Whelan, J.P., Borkholder, D.A., Ma, W., Stenger, D.A., 1999. Development and application of cell-based biosensors. Ann. Biomed. Eng. 27, 697–711.

Radke, S.M., Alocilja, E.C., 2005. A high density microelectrode array biosensor for detection of E. coli O157:H7. Biosens. Bioelectron. 20, 1662–1667. https://doi.org/10.1016/j.bios.2004.07.021.

Ramis, G., Martínez-Alarcón, L., Quereda, J.J., Mendonça, L., Majado, M.J., Gomez-Coelho, K., Mrowiec, A., Herrero-Medrano, J.M., Abellaneda, J.M., Pallares, F.J., Ríos, A., Ramírez, P., Muñoz, A., 2013. Optimization of cytotoxicity assay by real-time, impedance-based cell analysis. Biomed. Microdevices 15, 985–995. https://doi.org/10.1007/s10544-013-9790-8.

Schneider, G., Burridge, K., 1994. Formation of focal adhesions by osteoblasts adhering to different substrata. Exp. Cell Res. 214, 264–269. https://doi.org/10.1006/excr.1994.1257.

Stolwijk, J.A., Matrougui, K., Renken, C.W., Trebak, M., 2015. Impedance analysis of GPCR-mediated changes in endothelial barrier function: overview and fundamental considerations for stable and reproducible measurements. Pflug. Arch. 467, 2193–2218. https://doi.org/10.1007/s00424-014-1674-0.

Thomas Jr, C.A., Springer, P.A., Loeb, G.E., Berwald-Netter, Y., Okun, L.M., 1972. A miniature microelectrode array to monitor the bioelectric activity of cultured cells. Exp. Cell Res. 74, 61–66.

Tiruppathi, C., Malik, A.B., Del Vecchio, P.J., Keese, C.R., Giaever, I., 1992. Electrical method for detection of endothelial cell shape change in real time: assessment of endothelial barrier function. Proc. Natl. Acad. Sci. USA 89, 7919–7923.

Triplett, J.W., Pavalko, F.M., 2006. Disruption of α-actinin-integrin interactions at focal adhesions renders osteoblasts susceptible to apoptosis. Am. J. Physiol.-Cell Physiol. 291, C909–C921. https://doi.org/10.1152/ajpcell.00113.2006.

Watterson, D., Robinson, J., Chappell, K.J., Butler, M.S., Edwards, D.J., Fry, S.R., Bermingham, I.M., Cooper, M.A., Young, P.R., 2016. A generic screening platform for inhibitors of virus induced cell fusion using cellular electrical impedance. Sci. Rep. 6, 22791. https://doi.org/10.1038/srep22791.

Wegener, J., Keese, C.R., Giaever, I., 2000. Electric cell–substrate impedance sensing (ECIS) as a noninvasive means to monitor the kinetics of cell spreading to artificial surfaces. Exp. Cell Res. 259, 158–166. https://doi.org/10.1006/excr.2000.4919.

Wyllie, A.H., Kerr, J.F.R., Currie, A.R., 1980. Cell death: the significance of apoptosis. In: Bourne, G.H., Danielli, J.F., Jeon, K.W. (Eds.), International Review of Cytology. Academic Press, pp. 251–306. https://doi.org/10.1016/S0074-7696(08)62312-8.

Xu, Y., Xie, X., Duan, Y., Wang, L., Cheng, Z., Cheng, J., 2016. A review of impedance measurements of whole cells. Biosens. Bioelectron. 77, 824–836. https://doi.org/10.1016/j.bios.2015.10.027.

Yeon, J.H., Park, J.-K., 2005. Cytotoxicity test based on electrochemical impedance measurement of HepG2 cultured in microfabricated cell chip. Anal. Biochem. 341, 308–315. https://doi.org/10.1016/j.ab.2005.03.047.

Zhu, Z., Frey, O., Haandbaek, N., Franke, F., Rudolf, F., Hierlemann, A., 2015. Time-lapse electrical impedance spectroscopy for monitoring the cell cycle of single immobilized S. pombe cells. Sci. Rep. 5, 17180. https://doi.org/10.1038/srep17180.